# Uncertainty Analysis in the Inverse of Equivalent Conductance Method for Dealing with Crosstalk in 2-D Resistive Sensor Arrays

Javier Martinez-Cesteros, Carlos Medrano-Sanchez, *Senior Member, IEEE,* Inmaculada Plaza-Garcia, *Senior Member, IEEE,* Raul Igual-Catalan

***Abstract*— 2-D resistive sensor arrays (RSAs) appear in many applications to measure physical quantities in a surface. However, they suffer from a crosstalk problem when the simplest configuration is used to address a row-column. Thus, the value of a single cell cannot be measured directly. Several hardware solutions have been proposed to solve it totally or partially but all of them make the circuit more complex. In a previous paper we proposed an innovative numerical solution to eliminate crosstalk after a complete scan of the matrix, which is named in this paper as Inverse of Equivalent Conductance Method (IECM). In the current study, we have analyzed the implications of the method for the uncertainty of the calculated cell resistance by first deriving the sensitivity of the solution and then applying uncertainty propagation theory. The theoretical results have been tested in simulated arrays and in a real 6x6 RSA with known values of resistances with good agreement. The uncertainty analysis is able to predict which values are reliable. In general, the lowest resistances of the array are better solved by IECM as expected. In addition, it is also shown that IECM has the potential to be adapted to other hardware configurations that reduce crosstalk, helping to overcome some of its limitations.**

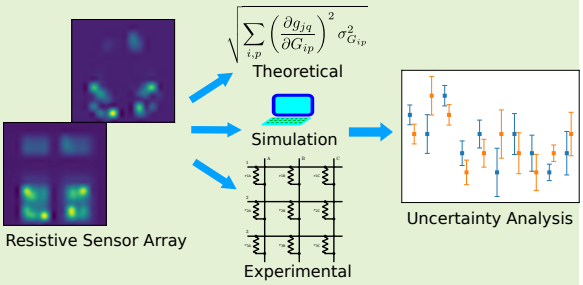


***Index Terms*— Resistive sensor array, Crosstalk, Uncertainty propagation, Piezoresistive sensor.**

## I. Introduction

WHEN a set of resistive sensor elements (cells) are placed in a matrix they form a 2-D resistive sensor array (RSA). This configuration can be used to perceive the associated physical magnitude in a surface. This set-up appears in many applications such as thermal imaging based on infrared sensors, electronic nose or pressure sensitive mats (PSM) [1].

To limit the number of connections, a single cell of the array is conventionally addressed using a row-column selection device (analog multiplexer/demultiplexer). However, the basic data acquisition configuration suffers from the problem of crosstalk [1], [2]: when a cell is addressed the current not only flows through it but also through other elements because row and column connections are shared. This alters largely the measurement. For PSMs the crosstalk is visually very apparent since there seems to be pressure exerted on regions where there are no objects on them. This is why this effect is sometimes called ghost effect. Several solutions have been proposed to solve the crosstalk problem partially or completely. They have been reviewed in [2]. For instance the Inserting Diode Method [2], [3] proposes inserting a diode in series with every sensitive element. Thus parasitic currents are blocked by the unidirectional conductivity of diodes. In the Zero Potential Method the non-scanned electrodes are set to zero potential [2], [4], [5]. This allows diverting the parasitic currents so that they do not pass through the measurement system. Several variants have been proposed by combining the use of 2:1 multiplexers, which can connect to ground a given electrode, and op-amps (OAs) in a negative feedback configuration, which can connect it to a virtual ground. For fast readout, one OA per output channel and an FPGA for parallel processing can be combined [6]. With ideal components both IDM or ZPM could remove the crosstalk effect completely. Both solutions have been adopted for PSMs: IDM in [7], [8] or ZPM [9], [10]. For non ideal components several modifications have been proposed, for instance using AC measurements [11], extending the matrix with a row and a column of known resistors [12] or modifying the ZPM configuration [13]. In the last two studies more measurements are required, but the cell resistances can be deduced from them taking into account non ideal components. These and other techniques have their

J. M. acknowledges a grant from the Spanish “Ministerio de Ciencia, Innovación y Universidades” FPU-18/04282. This work has been partially supported by “Departamento de Ciencia, Universidad y Sociedad del Conocimiento, del Gobierno de Aragón” (T49_20R). Corresponding author: Javier Martinez-Cesteros (javimzcs@unizar.es)

All the authors take part in the research team EduQTech, E.U. Politécnica, 44003 Teruel, University of Zaragoza, Spain (e-mail: {javimzcs, ctmedra, inmap, rigual}@unizar.es).

All the authours but the first are part of the IIS Aragón, University of Zaragoza, 50009 Zaragoza, Spain

Manuscript received XXXX.

advantages and disadvantages [2]. In general, more electronic components are required to solve the problem and the circuit complexity is larger.

In [14], [15] a software solution was proposed and tested with simulations and in a PSM to remove the ghost effect. Instead of avoiding the crosstalk problem directly, the proposed approach was to scan the complete matrix and then deduce the cell resistances from the set of values measured in the scan. This was grounded on the circuit analysis of the resistive array. In this paper we refer to this approach as Inverse of Equivalent Conductance Method (IECM). We note that it is slightly more convenient to work with conductances instead of resistances, but this is a minor point since knowing the conductance of a cell is equivalent to knowing its resistance. Although there were no analytical equation relating cell and measured conductances, several algorithms were proposed to find the cell conductance that best explain the measurements. One clear advantage of this software solution is that the circuit complexity can be kept to the minimum required. However, it has some drawbacks. For instance, for a 16x16 RSA each cell conductance is obtained from a set of 256 measured conductances by means of a rather complex algorithm. Since each measurement is inherently noisy, it is worth wondering whether the cell conductance value obtained in this way is reliable or not since it depends on many measurements. This is the question addressed in this paper. This kind of analysis is not very common in RSAs. In [13] the effect of output voltage noise was considered in simulations of a modified ZPM configuration and in [16] several sources of uncertainty were considered and estimated in some cases in direct interface solutions for reading RSAs. We think that this is an important point because IECM and other methods rely on a set of complex operations fed by a large set of measurements, so that the effect of noise could be amplified by them.

The goal of this paper is to determine the sensitivity of the cell conductances to the measured conductances in IECM. This allows a further objective: determining the uncertainty of the former by propagating the experimental uncertainty of the latter [17]. In this way, the reliability of cell conductances in a given experiment could be found and the user can be prevented when it is low. Up to our knowledge, there is no previous paper that addresses this issue and characterizes IECM from this practical point of view. The uncertainty we are dealing with arises from random effects, which originate from noise in voltage measurements. An additional contribution is to show that the ideas behind IECM can be extended to circuits different from the one shown in [14]. The code associated with this paper has been made publicly available [1].

The rest of the paper is organized as follows: section II summarizes the IECM approach, provides a comparison with recent methods for RSA scanning, and establishes how the sensitivity of cell conductances can be obtained, which is the key quantity to use uncertainty propagation. Section III shows the results obtained in simulations and in a 6x6 real RSA with known values of resistances for reference. The section compares the results of uncertainty propagation equation and the uncertainty obtained from simulations or experiments respectively. In section IV the main conclusions are drawn together with future lines of research. The appendix presents and adaptation of IECM to a recent proposed configuration that eliminates the main source of crosstalk using a hardware solution.

[1]Release v202110, https://gitlab.com/ctmedra1/inverse-of-equivalent-conductance-method/-/releases

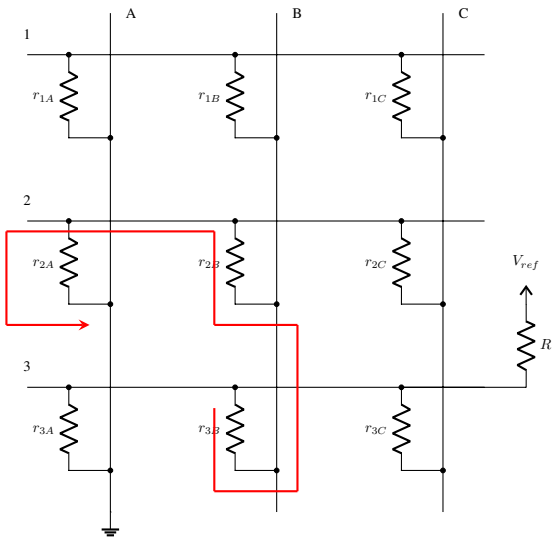


Fig. 1: Example of a 3x3 RSA: cell 3A is being addressed. The red line shows one of the current paths that do not pass through $r_{3A}$.

## II. Theoretical background

### A. The crosstalk problem in RSA and the IECM approach

For the sake of clarity, the IECM approach [14] is outlined in this subsection. The notation used through the paper is also introduced.

In an RSA, there is a set of resistive sensors configured in an array. Many signal conditioning circuits are configured by selecting a row-column and connecting them to the measurement circuit. A typical configuration is shown in figure 1, in which row 3 is connected to $V_{ref}$ via a resistor and column A to ground. Thus, a voltage divider circuit is formed with the aim of measuring $r_{3A}$ from the value of the voltage at node 3 (row 3 would be connected to an ADC for instance). However, the current not only flows through $r_{3A}$ and there are many paths for it as the one shown in red. In fact, the quantity that can be measured is not $r_{3A}$ but the equivalent resistance between nodes 3 and A, which we indicate as $R_{3A}$. In this paper we use the notation $r_{ip}/g_{ip}$ to refer to the resistance/conductance of a single cell located at row $i$ column $p$, and $R_{ip}/G_{ip}$ for the equivalent resistance/conductance between the same pair of nodes. Thus, the problem is to find the cell resistances, which are the quantities we are interested in, from the set of equivalent resistances, which are the quantities that can be obtained in the measurement.

From a formal point of view, the equivalent conductance between nodes 3 and A can be found by solving the circuit of

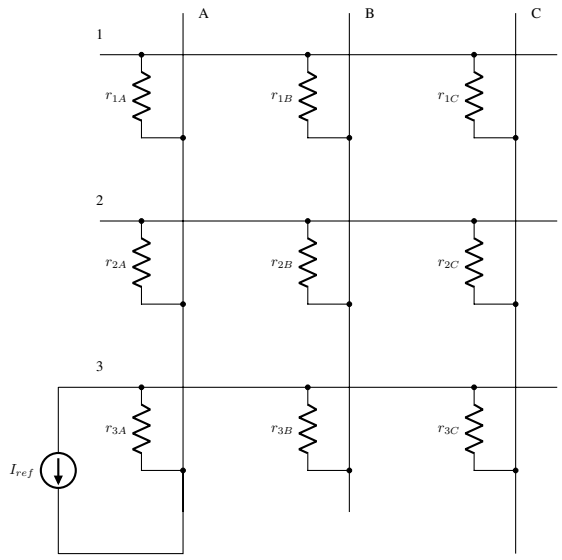


Fig. 2: Theoretical circuit to determine the equivalent resistance between row 3 and column $A$ in a 3x3 array.

figure 2 in which a current is injected between them. Given that there is a different circuit for each row-column pair, we introduce the following notation: $V_{ip,j}$ refers to the voltage at node $j$ in the circuit used to find the equivalent resistance value between row $i$ and column $p$. Once the circuit is solved, the equivalent conductance is $G_{3A} = \frac{I_{ref}}{V_{3A,A} - V_{3A,3}}$ or, in general:

$$G_{ip} = \frac{I_{ref}}{V_{ip,p} - V_{ip,i}} \tag{1}$$

$I_{ref}$ is just a multiplicative constant in the circuit solution that can be set to 1 in the implementation.

Without loss of generality, we consider row 1 as ground. The circuit for row $i$ and column $p$ can be solved using Kirchoff's laws that lead to a linear system equation:

$$\mathbf{C}\mathbf{V}_{ip} = \mathbf{I}_{ip} \tag{2}$$

where the matrix $\mathbf{C}$ has physical dimension of conductance, and the notation $\mathbf{V}_{ip}$ refers to the voltage solution in vector form and $\mathbf{I}_{ip}$ to the current injected in vector form.

For instance in the circuit shown in figure 2 , the nodes are ordered as: 2, 3, $A$, $B$, $C$. Thus, the matrix $\mathbf{C}$ is:

$$\mathbf{C} = \begin{pmatrix} g_{2,} & 0 & -g_{2A} & -g_{2B} & -g_{2C} \\ 0 & g_{3,} & -g_{3A} & -g_{3B} & -g_{3C} \\ -g_{2A} & -g_{3A} & g_{,A} & 0 & 0 \\ -g_{2B} & -g_{3B} & 0 & g_{,B} & 0 \\ -g_{2C} & -g_{3C} & 0 & 0 & g_{,C} \end{pmatrix} \tag{3}$$

where the shorthand notations $g_{i,} = \sum_p g_{ip}$ and $g_{,p} = \sum_i g_{ip}$ have been used. For instance: $g_{3,} = g_{3A} + g_{3B} + g_{3C}$.

Finally, the vector $\mathbf{I}_{3A}$ would be $\mathbf{I}_{3A} = (0, -I_{ref}, I_{ref}, 0, 0)^T$.

It should be noted that the matrix $\mathbf{C}$ does not depend on the row-column pair under consideration in equation 2. It is the corresponding intensity vector, $\mathbf{I}_{ip}$, the quantity that reflects the row-column nodes connected by the current source.

Therefore, if the cell conductances are known, the equivalent conductances can be found with the following steps for each row-column pair:

- Solving the circuit to find the equivalent resistance value of the row-column pair under consideration (similar to figure 2).
- Applying equation 1.

The general relation between those two sets of conductances is represented in a short notation as $\mathbf{G} = \mathbf{F}(\mathbf{g})$ and each component is denoted as $G_{ip} = F_{ip}(\mathbf{g})$. In [14] we proposed a software solution that aims to invert the relation, that is, formally to do the following operation:

$$\mathbf{g} = \mathbf{F}^{-1}(\mathbf{G}) \tag{4}$$

In this paper, we call this approach the Inverse of Equivalent Conductance Method (IECM). In [14] several numerical algorithms have been proposed to solve this inverse relation. In particular, in this paper we consider the solution based on a least-squares approach. The elements of $\mathbf{g}$ can be found by minimizing the following cost function:

$$\|\mathbf{G}_{exp} - \mathbf{F}(\mathbf{g})\|^2 = \sum_{i,p} \|G_{exp,ip} - F_{ip}(\mathbf{g})\|^2 \tag{5}$$

The cell conductances are also subjected to an additional constraint $0 \leq g_{ip}$. In equation 5, $G_{exp,ip}$ are the quantities measured after a complete scan of the RSA.

### B. Qualitative comparison of IECM with other methods

The purpose of this subsection is to give a context of IECM within the broad range of solutions given in the literature to solve the crosstalk problem in RSAs. Advantages and disadvantages of IECM will be outlined in comparison with state of the art methods.

For an RSA it is not practical to let each cell to be read through its own lines. Thus, a set of row and column lines addresses the array and have to be scanned. The role of rows and columns could be interchanged but we consider in this paper that, generally speaking, the scanning is performed by powering a row and then reading the columns at once (parallel readout mode) or sequentially (single readout mode). The matrix size is denoted as $N_R \times N_C$. Thus, in parallel readout mode a single row is addressed each time and all the columns are read in parallel. In a typical configuration [4], the selected row is connected to a given voltage, $V_{ref}$, and all the others to ground. The columns are connected to OAs with a negative feedback resistor whose value can be set to provide the desired output range for an expected input range of sensor resistances. The negative node acts as a virtual ground. This is the basis of ZPM. For ideal components, it eliminates the primary crosstalk in the array. Buffers or switches can be used to select rows, sometimes together with voltage followers. In turn, every column needs an OA and the corresponding ADC. The combination of capacitive feedback and an FPGA is an alternative to perform several conversions simultaneously [6]. However, if the components are not ideal there is still some remaining crosstalk. The non ideal behavior includes: output

TABLE I: Comparison of methods.

| Method | Readout Time | Readout Mode | # Op Amp | Selection Components | # Control Lines | Current |
|---|---|---|---|---|---|---|
| IIDFCC [18] | $2 \cdot (N_R \cdot N_C)$ | Single | 1 | $N_R + N_C$ (2:1 MUX) | $N_R + N_C$ | $V_{ref}/R'$ |
| QZPM [13] | $N_C \cdot (N_R + (N_C + 1)/2) + N_R$ | Single | 1 | $N_R + N_C$ (2:1 MUX) | $N_R + N_C$ | $< V_{ref}/R$ |
| proposed | $N_R \cdot N_C$ | Single | 0 | 1 ($N_R$:1 MUX) + 1 ($N_C$:1 MUX) | $log_2(N_R \cdot N_C)$ | $< V_{ref}/R$ |
| Improved ZPM-I [12] | $N_R$+1 | Parallel | $N_C$+1 | $N_R$+1 Buffer | $N_R$+1 | $V_{ref}/R'$ |
| Improved ZPM-II [12] | $N_R$+2 | Parallel | $N_C$+1 | $N_R$+1 Buffer | $N_R$+1 | $V_{ref}/R'$ |

$R$ is a known resistor set by the designer that limits the current and $R'$ is the series between the output resistance of the buffer and the equivalent resistance of the RSA.
$R'$ can be low, so that power can be high in the first and in the last 2 methods presented in the table. Buffer role can also be played by switches or 2:1 MUX.

resistance of buffer or switches, offset voltage, bias current, and finite gain of OAs. These issues were addressed in [12], [19]: by adding a row and a column with known resistors, it is shown that the cell resistances can be obtained from a combination of measured output voltages that eliminates the effect of non ideal components. The disadvantage of parallel readout methods is the number of components required to implement them: buffer or switches, each one with its own control line, and the number of OAs and ADCs. Thus, the size and complexity of the circuit can become large. Power can also be an issue, not only because of the power required by the components, but also because cell resistances are connected between $V_{ref}$ and ground in the typical configurations, so that the current is limited only by their value and the resistance of the buffer or switch. An additional limiting resistance per row could be set to reduce power. However, if the designer has no constraints on power, size, cost and space, a parallel readout mode is the best solution, achieving also the highest sampling rate. In this case there would be no need to perform a post-processing such as IECM to remove crosstalk.

On the other hand, if the readout mode is single, the number of components is reduced at the expense of increasing the scanning time. For a given row selected, each column must be selected too in this mode. The Voltage Feedback Method (VFM) [20] tries to set the same voltage level in the terminals of cells in the rows that are not being addressed. In this way, no current will flow through them and the primary crosstalk is eliminated. An OA together with a voltage divider circuit sets the same voltage at the input of non addressed rows as in the output of the selected column. The current in the non-selected columns of the selected row is diverted through the OA. Again, the non ideal behavior of components generates relevant errors. Thus, some modifications have been proposed like the Improved Isolated Drive Feedback Circuit with Compensation (IIDFCC) [18]: a suitable selection of resistor values in the voltage divider circuit (the average value of the internal MUX resistances) has been shown to greatly reduce the crosstalk effect due to the switch internal resistances. With respect to ZPM, it can be adapted to single mode readout. Each column requires a switch that can connect either to ground or to the OA. If the components were ideal this solution would remove crosstalk. However, the non ideal behavior is often relevant and large errors can appear. Hidalgo et al. [13] proposed a modification called Quasi Zero Potential Method (QZPM) in which row and column switches connect either to ground or to the so-called connecting node, which in turn connects to an OA configured as an inverter amplifier. In QZPM the RSA is in fact powered only through the voltage at the positive input of the OA, which establishes the same potential (ideally) at the negative input node. It is shown that the cell resistances can be deduced taking into account the effect of the internal switch resistance, $R_m$, after an extended set of measurements has been performed: either row-column pairs ($N_R \cdot N_C$ measurements), a single column ($N_C$ measurements), a single row ($N_R$ measurements), or pairs of columns ($N_C \cdot (N_C - 1)/2$ measurements) are connected to the connecting node. In comparison with the traditional ZPM method, the scanning time is larger but ZPM cannot cope with non ideal switches, $R_m \neq 0$, which give rise to errors.

Contrary to previous studies, IECM provides a software solution to the problem of crosstalk. The key point to apply IECM is to be able to measure the equivalent resistance of an RSA when a row-column pair is selected. In the circuit shown in figure 1 a voltage divider circuit is used, but a configuration with an OA is also possible. For the purpose of the current discussion, we focus on the voltage divider option. With respect to previous studies the configuration belongs to the group of single mode readout circuits. Table I presents a summary of characteristics of state-of-the-art methods. The voltage divider limits the current in the circuit, which is important in portable devices. This is in contrast to the original ZPM and VFM methods, or parallel readout methods [12]. With respect to QZMP, the proposed circuit has simpler and smaller components and less PCB paths. For instance, column selection requires an $N_C : 1$ MUX with their $log_2(N_C)$ control lines, while in QZMP $N_C$ analog switches are required, each one with its own control line. The switches are commonly named as single pole double throw switches or $2 : 1$ MUX. A similar consideration could be done for the rows. Thus, the proposed configuration is a minimal hardware solution. As for the manufacturing requirements of the acquisition circuit, it would allow reducing as much as possible the requirement of components and minimizing the number of control lines required. Even low-end microcontrollers are likely to have the required number of digital outputs. All together, this would lead to a data acquisition system of minimal cost and space. Besides, QZPM requires extra measurements compared with the traditional $N_R \cdot N_C$ readings and makes the system slower. However, in the circuit proposed the primary crosstalk is not eliminated, and the required post-processing is a set of complex operations from a large set of experimental values, which is sensitive to noise as we are going to show in the

experimental section of the paper. Anyway, the hardware requirements of QZPM are also low. It is up to the designer to decide if the decrease in circuit complexity and size of the kind of circuit shown in figure 1 is worth for a given application.

Given said that, in the appendix it is shown that IECM has the potential to be adapted to QZPM in a general framework of optimization methods. This shows that this kind of methods are worth to be studied for dealing with crosstalk in RSAs.

### C. Uncertainty propagation in IECM

In this section we discuss the following problem. If the measured quantities $\mathbf{G}$ have an uncertainty, then the solution found in equation 4 has an uncertainty too. The key quantities that have to be obtained to calculate the influence on $\mathbf{g}$ are the partial derivatives:

$$\frac{\partial g_{jq}}{\partial G_{ip}} \tag{6}$$

If the partial derivatives are known, the law of propagation of uncertainty [17] can be set as:

$$\sigma_{g_{jq}} = \sqrt{\sum_{i,p} \left( \frac{\partial g_{jq}}{\partial G_{ip}} \right)^2 \sigma_{G_{ip}}^2} \tag{7}$$

where the symbol $\sigma_x$ is used for the standard deviation of a given quantity $x$, as a measure of its uncertainty.

We have not obtained directly $\frac{\partial g_{jq}}{\partial G_{ip}}$. However, in the supplementary material of the article it is shown that:

$$\frac{\partial G_{ip}}{\partial g_{jq}} = \frac{(V_{ip,j} - V_{ip,q})^2}{(V_{ip,p} - V_{ip,i})^2} \tag{8}$$

The indices $(i, p)$ or $(j, q)$ refer to the physical row-column position in an RSA. For the purpose of the next reasoning, it is convenient to see $\mathbf{g}$ or $\mathbf{G}$ as single vectors, flattening the physical indices into a single mathematical index. Therefore, we represent the set of partial derivatives as $\frac{\partial \mathbf{G}}{\partial \mathbf{g}}$, which can be seen as a matrix. For instance, in a 16x16 RSA, there are 256 cell conductances and 256 equivalent conductances. Thus, the matrix $\frac{\partial \mathbf{G}}{\partial \mathbf{g}}$ is a 256x256 matrix representing the partial derivatives of each equivalent conductance with respect to each cell conductance. Following the theory of partial derivatives, the required quantities, $\frac{\partial \mathbf{g}}{\partial \mathbf{G}}$, can be obtained as:

$$\frac{\partial \mathbf{g}}{\partial \mathbf{G}} = \left( \frac{\partial \mathbf{G}}{\partial \mathbf{g}} \right)^{-1} \tag{9}$$

To sum up, the partial derivatives required in equation 7 can be obtained by first calculating the set of partial derivatives in equation 8, and then obtaining the inverse matrix, equation 9. It should be highlighted that all the voltages required in equation 8 are obtained when running IECM. Equation 7 also requires the quantities $\sigma_{G_{ip}}$. In this paper, we refer to them as the noise model. They represent the noise of the measurement system.

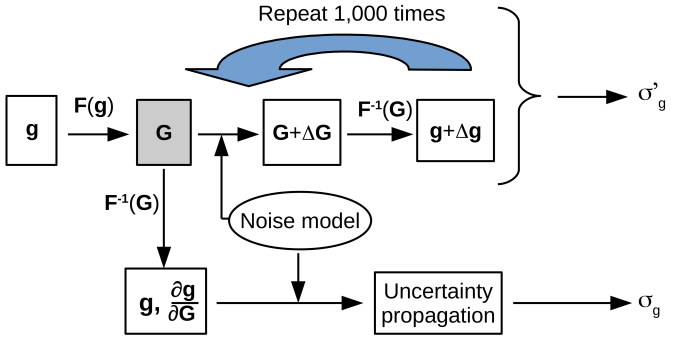


Fig. 3: Schematic view of the process to obtain uncertainty from simulations, $\sigma'_g$, and the comparison with uncertainty propagation equation, $\sigma_g$.

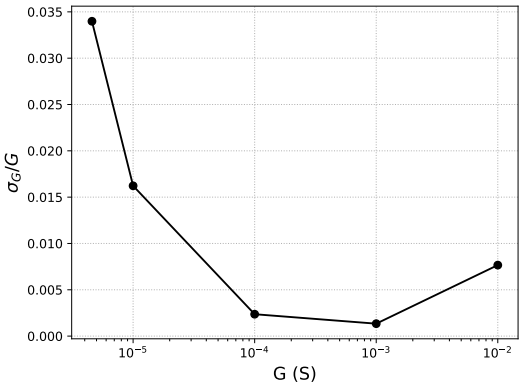


Fig. 4: Relative standard deviation of the noise model used.

## III. Results and Discussion

We present the results in two different contexts: one with simulated values and the other one with values measured from a real RSA.

### A. Simulated noise

The starting point of these simulations is a known value of an RSA ($\mathbf{g}$). Then $\mathbf{G}$ is calculated. Afterwards, we proceed by adding noise to $\mathbf{G}$ and using IECM to find $\mathbf{g}$ with a least-squares approach. This has been repeated $1,000$ times so that a value of standard deviation for each cell can be obtained [21]. These standard deviations can be compared with those obtained from the law of propagation of uncertainty. The general procedure carried out in this section is graphically explained in figure 3.

Although this section is entitled as "simulated noise", the noise model and some of the initial $\mathbf{g}$ are close to true values since they are taken from experiments (see section III-B). More specifically, the noise model corresponds to a gaussian distribution with relative standard deviation as shown in figure 4. In the figure the points correspond to measured noise in a real DAQ system for some known values of resistance. For intermediate values, linear interpolation has been used.

In the first case we present, the initial value of $\mathbf{g}$ is a set of 16x16 conductances randomly selected between $1e-5$

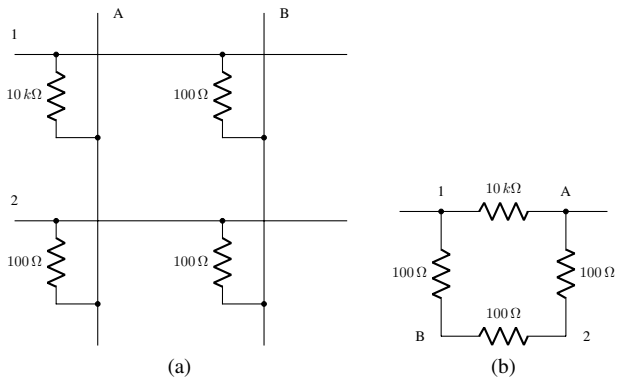


Fig. 5: a) Example of a 2x2 array; b) The equivalent resistor seen from nodes $(1, A)$.

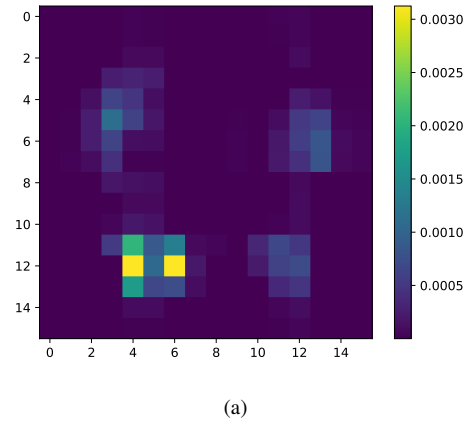


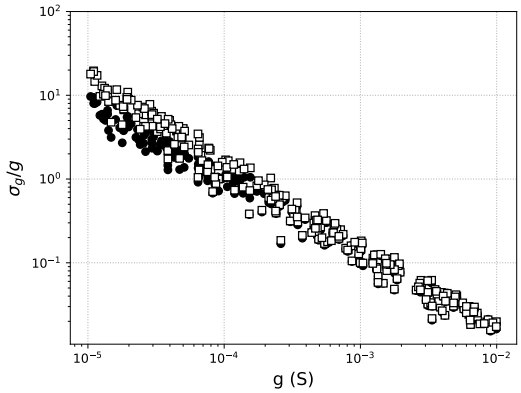


Fig. 6: Relative uncertainty as a function of conductance for a random array of conductances. Squares represent the values from uncertainty propagation equation, circles from simulation.

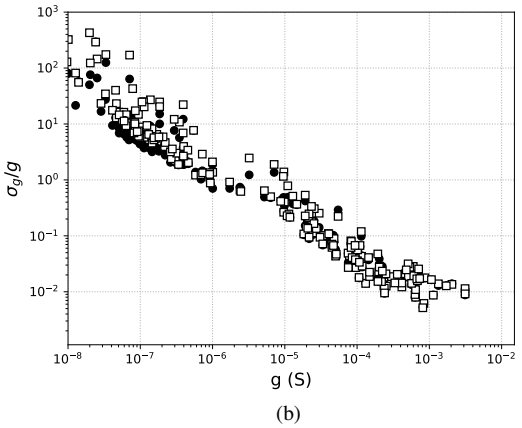


Fig. 7: Conductance map of a PSM (person in standing position, top figure), and relative uncertainty (bottom figure). Squares represent the values from uncertainty propagation equation, circles from simulation.

and $1e-2$ S. Figure 6 shows the relative noise figure for both, the simulations and the uncertainty propagation equation. For lower conductances, the uncertainty propagation equation tends to overestimate noise while for higher conductances it gives the same results as the simulations with ovelapping points in the figure. This behavior can be explained because equation 7 is not exact and comes from a linear approximation [17], [22]. Thus, it is not surprising that it deviates from true values in the range in which uncertainty is larger. In addition, the relative noise increases for low values of conductance, which are not reliable. It is not hard to imagine situations in which this can happen. For instance, let us consider a 2x2 array (figure 5a) composed of 10 kΩ in cell $(1, A)$ and three $100\,\Omega$ resistors in the other three cells. In this case, the equivalent resistance between nodes $1$ and $A$ is easily obtained as a parallel combination of 10 kΩ and $300\,\Omega$ (figure 5b), which is roughly $300\,\Omega$. For any other row-column pair the equivalent resistance would be the parallel combination of $100\,\Omega$ and $10,200\Omega$ using a similar reasoning. That value is about $100\,\Omega$. Therefore the largest resistor has little influence on the measurements and it is harder to be recovered from them.

In the second case, the values of $\mathbf{g}$ come from the measurements of a Velostat-based PSM [14] with a person standing on it [2]. Figure 7 shows the conductance map and the results of the noise estimation. In this case the uncertainty propagation equation and the simulation give almost the same results, even though the former shows a tendency to overestimate uncertainty values in the very low conductance range. Low conductances are not reliable at all, while for conductances above a value about $1e-4$ the uncertainty is less than $10$ % (in other words, resistances lower than a few kΩ can be recovered with that precision).

In the third case, the values of $\mathbf{g}$ come from the same PSM with a person in semi-tandem stance. In this case, the values of conductance before processing showed a clear ghost effect, while after the processing there is almost no pressure in the top right part, figure 8a, where no foot is in contact with the mat. The results are similar to the previous case but with some

[2]Data come from a stability analysis experiment. The protocol was conducted according to the guidelines of the Declaration of Helsinki, and approved by the regional ethics committee, Comité de Ética de la Investigación de la Comunidad Autónoma de Aragón (CEICA), protocol code: 22/2019, protocol version: 1.0, 29-11-2019, date of approval: December $18^{th}$, 2019.

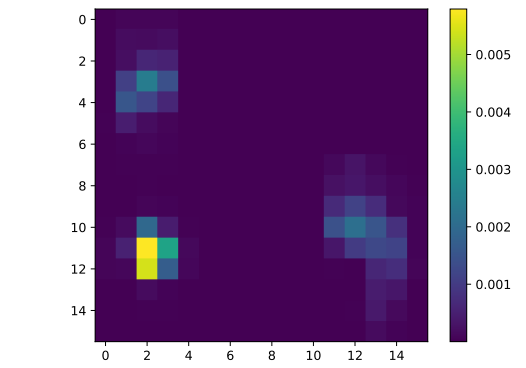


(a)

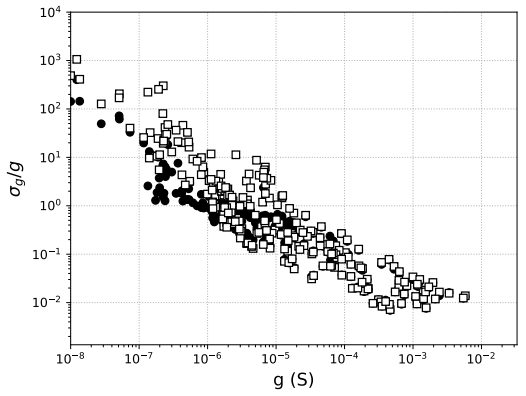


(b)

Fig. 8: Conductance map of a PSM (person in semi tandem, top figure), and relative uncertainty (bottom figure). Squares represent the values from uncertainty propagation equation, circles from simulation.

minor differences: The spread of the values seems larger in this case and the tendency for uncertainty overestimation of equation 7 is even more clear.

### *B. Noise in a real RSA*

In this case, we built a PCB with a female socket to plug resistors. The connections reproduced a 6x6 RSA. The PCB has also a connector to plug a DAQ system. It is based on analog multiplexers to select row-column pairs, a voltage divider circuit, a microcontroller to read analog values and a bluetooth module to send values to a PC. It is very similar to others described in the literature [14], [23], [24]. The block diagram is shown in figure 9. CD74HC4067 analog multiplexers were used to select the row and colums. The microcontroller used for the sampling and sending process was a STM32F103C8T6 (ARM® Cortex® M3, 32bits, 72MHz), which embeds a SAR switched-capacitor ADC (12 bits). The microcontroller communicates with an HC-05 Bluetooth module, which sends data to a PC. The whole RSA can be sampled at 10 Hz.

The first step was to determine the noise model. For that

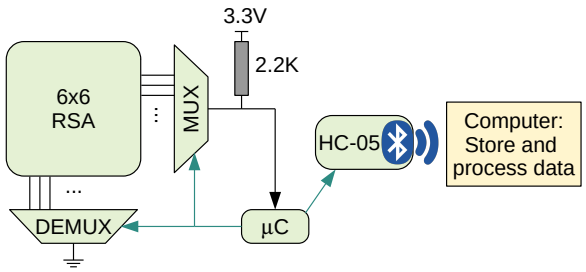


Fig. 9: Block diagram of the acquisition system.

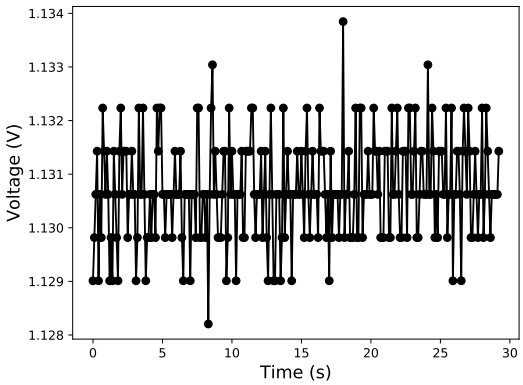


Fig. 10: Measured voltage for a test resistor of 1 kΩ showing the noise level in the system.

purpose, a known single test resistor was placed in a cell and the rest of connections were left open. In this way, an ideal situation was achieved: measuring the equivalent resistance was the same as measuring the cell resistance, all other being infinite. Then, we acquired data for about 30 s (300 samples) and extracted the standard deviation. An example of the voltage values measured for a test resistor of 1 kΩ is presented in figure 10. Discrete jumps are clearly seen, corresponding to changes in the ADC readings of a few units. The global results are shown in table II for each value of resistance. It can be seen that the noise is almost constant, around $\pm 1$ mV. This corresponds to about $\pm 1.24$ LSB in the system. Therefore, it seems that the intrinsic quantification error is a large portion of the uncertainty in the system. It is likely that the noise would be larger in another environment but, given that our system is composed of a simple PCB and that it was not tested in a noisy environment, the measured noise may be lower than the typical value found on microcontroller applications. The results presented in figure 4 are derived from the values in table II just by expressing them in relative terms.

Once determined the noise model, we measured the noise with different configuration of the 6x6 RSA using resistors of 100 Ω, 1 kΩ, 10 kΩ and 100 kΩ. The procedure to obtain the experimental uncertainty and the estimation obtained from the uncertainty propagation equation is very similar to the one shown in figure 3. The difference is that instead of adding noise in the computer to an initial $\mathbf{G}$, in this section we just took several measurements of the same configuration in static conditions (about 30 s, 300 samples), getting several $\mathbf{G}$ values

TABLE II: Measured voltage noise level for various test resistors and the associated uncertainty in the conductance deduced from the voltage divider circuit. The noise is characterized in terms of standard deviations ($\sigma_v$ for voltage, $\sigma_g$ for conductance).

| Resistance Ω | $\sigma_v$ (mV) | $\sigma_g$ (S) |
|---|---|---|
| 100 | 1.0 | 7.7e-5 |
| 1,000 | 0.9 | 1.3e-6 |
| 10e3 | 1.1 | 2.4e-7 |
| 100e3 | 1.1 | 1.6e-7 |
| 220e3 | 1.1 | 1.6e-7 |

and then several values of $\mathbf{g}$ using IECM. In this way the experimental uncertainty could be determined. On the other hand, from a value of $\mathbf{G}$ (in fact, we took the median), we derived $\mathbf{g} = \mathbf{F}^{-1}(\mathbf{G})$ using IECM and the derivatives $\frac{\partial \mathbf{g}}{\partial \mathbf{G}}$, from which uncertainty propagation can be applied to obtain the expected uncertainty.

Two different configurations were tested. In the first configuration, the resistors were randomly selected, see figure 11a. In the second configuration we tested a case with a strong ghost effect, in which three corners are filled with 100 Ω resistor and the rest with higher values (figure 12a). The general trend of the results is similar to the cases shown in section III-A. However a graph like figures 7b and 8b is not very helpful because the points overlap due to the presence of a discrete set of resistance values. Therefore in this section, we represent only bar plots showing the cell values that can be determined with a relative precision better or close to 10%. They correspond to 100 Ω and 1 kΩ resistors. The bar plots in figures 11b and 12b show the value of conductance and the relative uncertainty obtained from the measurements and from the uncertainty propagation equation. In general, they agree reasonably well with some tendency to overestimation for 1 kΩ resistors ($1e-3$ S conductance) and underestimation for 100 Ω resistors ($1e-2$ S conductance) in the case in which there is strong ghost effect.

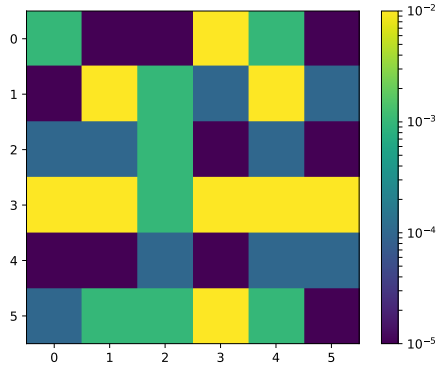


(a)

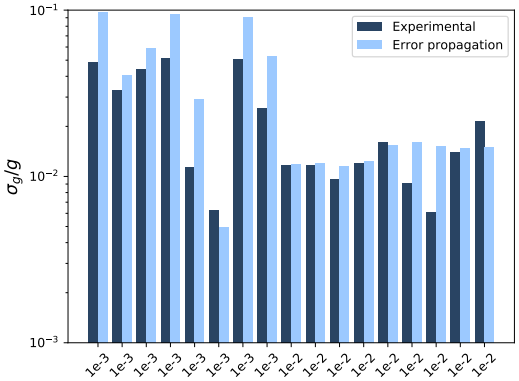


(b)

Fig. 11: Conductance map of a 6x6 RSA with random resistances (top) and relative uncertainty of the highest conductance cells (bottom), in which dark blue is the experimental uncertainty and the light blue the value obtained from the uncertainty propagation equation. Labels in x-axis represent the conductance in S of the corresponding cells.

## IV. Conclusions

In this paper we have proven an equation to find the sensitivity of cell conductances $\mathbf{g}$ with respect to equivalent conductance measurements $\mathbf{G}$ in an RSA when using IECM to eliminate the crosstalk problem. This leads to the possibility of estimating the uncertainty using the law of uncertainty propagation. We have tested this with simulated and real RSA. The uncertainty propagated is very close to the simulated and experimental ones for low values of resistance, which are the ones that can be obtained with a reasonable reliability. For higher resistances, the propagation equation tends to overestimate the uncertainty, but the main outcome is clear: they cannot be obtained reliably.

IECM is a software solution to the problem of crosstalk in RSAs. It has an advantage in terms of reduction of electronic components, which is very important for large arrays. A consequence of the results of this paper is that the largest resistance values cannot be obtained in this way reliably, while the lowest resistance values present far less uncertainty. The importance of this characteristic of IECM depends on the application. For a PSM, the uncertainty in large values of resistance (low values of conductance) does not imply too much change in terms of pressure exerted on the mat. This is due to the approximate proportionality between conductance and pressure in many sensitive materials. It would be rather irrelevant to find a center of pressure or an object shape. Nevertheless, this might not be the case for other sensors that are based on an RSA model. With the extension of IECM proposed in this paper, it can detect the situations in which the results are not reliable.

To apply the uncertainty propagation equation a noise model is required. In the experimental case, we built a 6x6 RSA on a PCB with a socket that allowed us to measure it in an easy way. For other configurations, it is unclear whether a realistic noise model can be found because it should be measured as close as possible to the final set up to account for factors such as long PCB traces. Another option could be to consider the noise model as a free parameter, instead of considering it as an a priori knowledge. Thus, the noise model that better

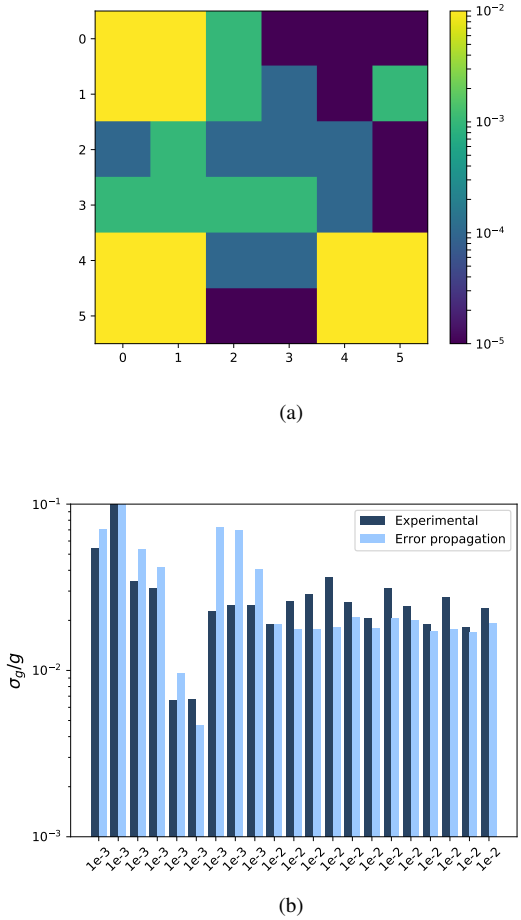


(a)

(b)

Fig. 12: Conductance map of a 6x6 RSA (top) that would show strong ghost effect if not corrected and relative uncertainty of the highest conductance cells (bottom), in which dark blue is the experimental uncertainty and the light blue the value obtained from the uncertainty propagation equation. Labels in x-axis represent the conductance in S of the corresponding cells.

explains the experimental uncertainty based on the uncertainty propagation could be selected in a kind of fitting approach. This option will be investigated in the future.

## ADAPTATION OF IECM TO QZPM

In this appendix we are going to show an example of the adaptation of IECM to other circuit configurations. In particular, we are going to adapt it to the kind of circuit shown in figure 13a corresponding to QZPM. It was proposed by Higalgo et al. [13]. It is a configuration derived from ZPM for sequential reading with few components. The switches can connect any row or column either to ground or to node $V_{in}$, the so-called connecting node. In figure 13b the simultaneous connection of a row and a column is presented including the internal non zero switch resistances. It has been shown that a series of voltage measurements on the circuit output allows calculating cell conductances without the crosstalk due to non ideal switches. For an $N_R \times N_C$ matrix, the readings required are associated to different configurations of connections to the connecting node: i) column-row pairs ($N_R \cdot N_C$); ii) Only a single row at a time ($N_R$); iii) Only a single column at a time ($N_C$); iv) Different pairs column-column ($N_C \cdot (N_C - 1)/2$).

However, an assumption of QZPM is that the internal resistance of the switch is known and the same for all the components, $r_i = r^p = r_s$, where we have used the notation $r_i/r^p$ for the internal resistance of the switch in row $i$/column $p$. The associated conductances are denoted as $g_i$ and $g^p$. In this appendix, IECM is extended to the case in which the resistance is not known and even different for each switch. It is a more realistic situation because manufacturers provide typical values but it would be hard to know them for a particular set of components unless a calibration procedure is devised.

For a given configuration of the switches when the row $i$ and the column $p$ are connected to the connecting node, the output voltage is measured, $V_o(i,p)$. The following convention is used: if either $i = 0$ or $p = 0$ it means that there is no row or column connected to it respectively. The equivalent conductance of the network between the connecting node and ground can be obtained by considering an ideal OA (figure 13b). Firstly, the intensity that flows into the network, $I_{in}$, and the voltage at the connecting node, $V_{in}$ can be calculated as:

$$I_{in}(i,p) = \frac{V_o(i,p) - V_{ref}}{r_f} \tag{10}$$

$$V_{in}(i,p) = V_{ref} - I_{in}(i,p) \cdot r_d \tag{11}$$

Then, the equivalent conductance of the network for that particular configuration is:

$$G_{exp,ip} = \frac{I_{in}(i,p)}{V_{in}(i,p)} \tag{12}$$

Thus, a set of equivalent conductances, which we denote globally as $\mathbf{G}_{exp}$, can be obtained experimentally from the set of measured voltages for different switch configurations.

On the other hand, if the set of conductances in the array and in the switches were known, another set of equivalent conductances could be obtained by solving Kirchoff's laws in the corresponding configuration. For instance, formally the equivalent conductance can be obtained from the kind of circuit shown in figure 14 for a 3x3 array. There are $N_R + N_C + 1$ nodes in the circuit, corresponding to row voltages, $V_i$, column voltages, $V^p$, and the connecting node $V_{in}$. If row $i$ and column $p$ are connected to the connecting node through the switches, then the equations to be solved are:

$$g_j(V_j - V_{in}\delta_{ji}) + \sum_{q=1}^{N_C} g_{jq}(V_j - V^q) = 0 \tag{13}$$

for row nodes $j = 1, \ldots, N_R$,

$$g^q(V^q - V_{in}\delta_{qp}) + \sum_{j=1}^{N_R} g_{jq}(V^q - V_j) = 0 \tag{14}$$

for column nodes $q = 1, \ldots, N_C$, and

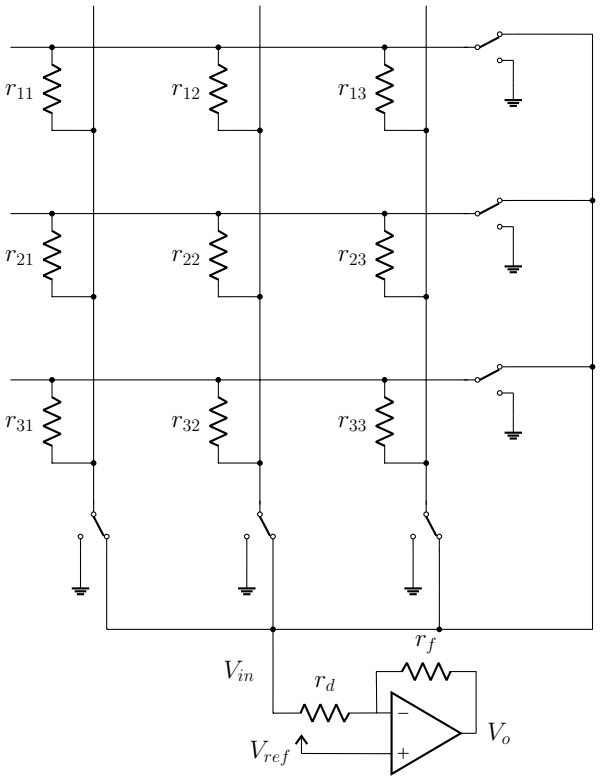


Fig. 13: (a) Circuit configuration of QZPM for a 3x3 array; (b) Example when row 1 and column 2 are connected to $V_{in}$ (internal resistance of the switches included).

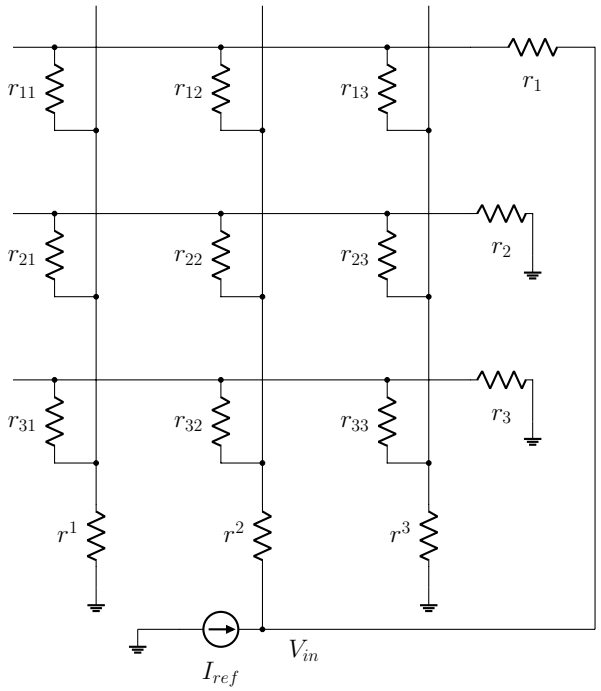


Fig. 14: Theoretical circuit to find the equivalent resistance of a 3x3 array when row 1 and column 2 are connected to the connecting node.

$$\sum_{j=1}^{N_R} \delta_{ij} g_j (V_{in} - V_j) + \sum_{q=1}^{N_C} \delta_{qp} g^q (V_{in} - V^q) = I_{ref} \quad (15)$$

for the connecting node.

In equations 13, 14 and 15, $\delta_{nm}$ is the Kronecker delta (1 if $n = m$, 0 otherwise). The notation is a bit succint but allows considering the following cases: a row-column pair, a single row, or a single column connected to $V_{in}$. For instance, if $i = 0$, which means that there is no row connected to $V_{in}$, then $\delta_{ji}$ is always zero in equation 13. This effectively removes $V_{in}$ from the equation according to the lack of connection. The current injected, $I_{ref}$, is just a multiplicative constant and can be set to 1 in the implementation.

We note that the number of unknown parameters is $N_R \cdot N_C + N_R + N_C$. Therefore, for the adaptation of IECM only the row-column pairs, the single column and the single row connections were taken into account. The column-column connection readings were not required. If they were two columns, $p_1$ and $p_2$, connected to $V_{in}$, then the substitution of $\delta_{qp}$ by $\delta_{qp_1} + \delta_{qp_2}$ in equations 14 and 15 would be enough to get the right equations in this case.

Once equations 13, 14 and 15 are solved, the equivalent conductance can be found as:

$$G_{ip} = \frac{I_{ref}}{V_{in}} \quad (16)$$

To sum up, a formal relation between the set of conductances, denoted globally as $\mathbf{g}$, and the set of equivalent conductances, $\mathbf{G}$, can be deduced using the algorithm in figure 15. This relation is denoted $\mathbf{G} = \mathbf{F}(\mathbf{g})$ in short.

**Input**: cell conductances $g_{jq}$, row switch conductances, $g_j$ and column switch conductances, $g^q$ with $j = 1, \cdots, N_R$ $q = 1, \cdots, N_C$
**Output**: Equivalent conductances $G_{ip}$, with $i = 0, \cdots, N_R$ $p = 0, \cdots, N_C$ for the configuration in which row $i$ and column $p$ are connected to the connecting node (0 index means no connection):
**for all** pairs $(i, p)$ except $(0, 0)$ **do**
  Solve equations 13, 14 and 15
  $G_{ip} \leftarrow \frac{I_{ref}}{V_{in}}$
**end for**

Fig. 15: Algorithm to find equivalent conductances for several configurations of the network.

The numerical relation between $\mathbf{g}$ and $\mathbf{G}$ allows stating the problem of finding the unknown conductances as an optimization problem. The elements of $\mathbf{g}$ are found by minimizing the following cost function:

$$\|\mathbf{G}_{exp} - \mathbf{F}(\mathbf{g})\|^2 \tag{17}$$

subject to the constraints:

$$0 \leq g_{ip},\ 0 \leq g_i,\ 0 \leq g^p \tag{18}$$

To test the adaptation of IECM to QZPM we have considered a set of simulations. For different arrays sizes, random arrays of sensor resistances were obtained in the range $100\,\Omega$-$10\,k\Omega$. The resistances of the switches were also randomly distributed in the ranges $10 \pm 5\,\Omega$ or $10 \pm 1\,\Omega$. Firstly, the procedure explained in figure 15 was applied to extract the equivalent conductances, which play the role of $\mathbf{G}_{exp}$ (in other words, an ideal set of experimental values). Then, we applied a least square approach to solve the minimization of the objective function 17 and to test if the cell conductances could be recovered. Two kinds of simulations were performed. On the one hand, a set of simulations were run with circuits having a single unknown switch resistance, the same for all the switches. In the implementation we forced $g_i = g^p = g_s$, a single parameter to be optimized other than the sensor matrix itself. On the other hand, we considered circuits in which each $g_i$ and $g^p$ was allowed to take its own value ($N_R + N_C$ additional free parameters).

Moreover, we also implemented the equations of QZPM [13] considering an ideal OA (equations 10 and 11) with $r_d = 100\,\Omega$, $r_f = 400\,\Omega$ and $V_{ref} = 1\,V$. QZPM assumes the same internal resistance for all the switches, which we took as $10\,\Omega$. In this way we could check the output of QZPM when the assumption is not true. The values of resistances are also taken from typical values shown in [13].

If the solution found by an algorithm for a cell is denoted as $g'_{ip}$, the absolute relative error (ARE) was obtained as:

$$\epsilon_{ip} = \left| \frac{g'_{ip} - g_{ip}}{g_{ip}} \right| \tag{19}$$

Ten simulations were repeated for each of the conditions considered above. The values of the ARE 95th percentile are reported in tables III and IV for a single switch resistance (the same for all the switches) or for $N_R + N_C$ different switch resistances respectively. For QZPM a range of $\pm 1\,\Omega$ in $10\,\Omega$ induces errors in the system above 4%. The error increases with the size of the array. If the internal resistance range is $\pm 5\,\Omega$ the situation is even worse. On the other hand, IECM is able to recover cell values with high accuracy.

TABLE III: ARE for the adaptation of IECM to QZPM and the original QZPM implementation. The 95th percentile across all the simulation is provided. All the switches have the same resistance value, $r_s$, which was varied in two different ranges. QZPM assumed a fixed value ($10\,\Omega$).

| | Range $r_s = 10 \pm 5\Omega$ | | Range $r_s = 10 \pm 1\Omega$ | |
|---|---|---|---|---|
| | IECM | QZPM | IECM | QZPM |
| size | 95th PCTL | 95th PCTL | 95th PCTL | 95th PCTL |
| 4x4 | 1.9e-10 | 0.28 | 2.0e-10 | 4.5e-2 |
| 6x6 | 5.3e-10 | 0.35 | 1.8e-12 | 7.7e-2 |
| 8x8 | 2.6e-10 | 0.53 | 1.0e-12 | 0.10 |
| 10x10 | 6.9e-11 | 0.89 | 2.6e-12 | 0.12 |
| 12x12 | 1.7e-11 | 1.4 | 2.0e-11 | 0.13 |

TABLE IV: ARE for the adaptation of IECM to QZPM and the original QZPM implementation. The 95th percentile across all the simulation is provided. The switches in the circuit are allowed to have different values, which were varied in two different ranges. QZPM assumed a fixed value ($10\,\Omega$).

| | Range $r_s = 10 \pm 5\Omega$ | | Range $r_s = 10 \pm 1\Omega$ | |
|---|---|---|---|---|
| | IECM | QZPM | IECM | QZPM |
| size | 95th PCTL | 95th PCTL | 95th PCTL | 95th PCTL |
| 4x4 | 4.7e-5 | 0.19 | 5.9e-10 | 4.2e-2 |
| 6x6 | 3.4e-11 | 0.24 | 1.4e-11 | 4.6e-2 |
| 8x8 | 1.7e-4 | 0.37 | 5.0e-10 | 6.5e-2 |
| 10x10 | 8.7e-5 | 0.40 | 6.5e-11 | 7.9e-2 |
| 12x12 | 8.0e-6 | 0.75 | 8.7e-4 | 0.11 |

Nonetheless, comparing tables IV and III, it is clear that the IECM error is large when all the switch resistances are allowed to get a different value. This is likely to be related to the associated extra number of free parameters. It is known that optimization problems are much harder when the number of parameters increases and there might be several minima of the cost function. The errors for a particular simulation configuration are shown in figure 16 (10x10 array, every switch allowed to get its own internal resistance in the range $10 \pm 5\,\Omega$). No trend is visually seen with respect to the x-axis, except for a slight increase in the QZPM error for very low values of conductance. The IECM errors are mainly below $1e-9$, but some points reach higher values. They are responsible for achieving a 95th percentile value of $8.7e-5$, table IV. This fact also supports the idea that often the optimization algorithm ends at a point very close to the exact solution but that sometimes the distance to the solution is far larger, probably another minimum.

In conclusion, in our opinion it is worth studying numerical optimization methods within the context of crosstalk in RSA. They are more flexible and can overcome some of the assumptions of analytical methods. If the assumptions of the later are not fulfilled, relevant errors can appear in the system. In particular we have adapted IECM to QZPM when the internal resistance of the switches is not known. Other aspects such as

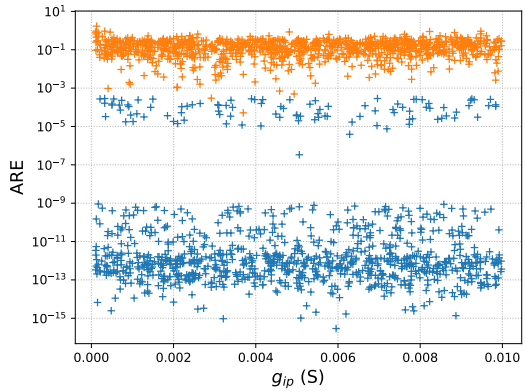


Fig. 16: ARE for a particular set of simulations: 10x10 array, every switch allowed to get its own internal resistance in the range $10 \pm 5\,\Omega$. Blue symbols refer to IECM, orange symbols to the original QZMP.

processing speed, effect of non-ideal OA, quantization error in ADC and noise were left out for future research because they are out of the scope of the present paper.

## REFERENCES


[1] R. S. Saxena, N. K. Saini, and R. K. Bhan, "Analysis of crosstalk in networked arrays of resistive sensors," *IEEE Sensors Journal*, vol. 11, no. 4, pp. 920–924, 2011.

[2] J. Wu, "Scanning approaches of 2-d resistive sensor arrays: A review," *IEEE Sensors Journal*, vol. 17, no. 4, pp. 914–925, 2017.

[3] W. E. Snyder and J. St. Clair, "Conductive elastomers as sensor for industrial parts handling equipment," *IEEE Transactions on Instrumentation and Measurement*, vol. 27, no. 1, pp. 94–99, March 1978.

[4] R. Lazzarini, R. Magni, and P. Dario, "A tactile array sensor layered in an artificial skin," in *Proceedings 1995 IEEE/RSJ International Conference on Intelligent Robots and Systems. Human Robot Interaction and Cooperative Robots*, vol. 3, 1995, pp. 114–119 vol.3.

[5] H. Liu, Y.-F. Zhang, Y.-W. Liu, and M.-H. Jin, "Measurement errors in the scanning of resistive sensor arrays," *Sensors and Actuators A: Physical*, vol. 163, no. 1, pp. 198–204, 2010. [Online]. Available: https://www.sciencedirect.com/science/article/pii/S0924424710003626

[6] O. Oballe-Peinado, F. Vidal-Verdú, J. A. Sánchez-Durán, J. Castellanos-Ramos, and J. A. Hidalgo-López, "Improved circuits with capacitive feedback for readout resistive sensor arrays," *Sensors*, vol. 16, no. 2, 2016. [Online]. Available: https://www.mdpi.com/1424-8220/16/2/149

[7] S. S. Suprapto, A. W. Setiawan, H. Zakaria, W. Adiprawita, and B. Supartono, "Low-cost pressure sensor matrix using velostat," in *2017 5th International Conference on Instrumentation, Communications, Information Technology, and Biomedical Engineering (ICICI-BME)*, Nov 2017, pp. 137–140.

[8] L. Xu, G. Chen, J. Wang, R. Shen, and S. Zhao, "A sensing cushion using simple pressure distribution sensors," in *2012 IEEE International Conference on Multisensor Fusion and Integration for Intellige nt Systems (MFI)*, Sep. 2012, pp. 451–456.

[9] J. F. Saenz-Cogollo, M. Pau, B. Fraboni, and A. Bonfiglio, "Pressure mapping mat for tele-home care applications," *Sensors*, vol. 16, no. 3, 2016. [Online]. Available: http://www.mdpi.com/1424-8220/16/3/365

[10] H. Wang, D. Zhou, and J. Cao, "Development of a skin-like tactile sensor array for curved surface," *IEEE Sensors Journal*, vol. 14, no. 1, pp. 55–61, Jan 2014.

[11] Z. Hu, W. Tan, and O. Kanoun, "High accuracy and simultaneous scanning ac measurement approach for two-dimensional resistive sensor arrays," *IEEE Sensors Journal*, vol. 19, no. 12, pp. 4623–4628, 2019.

[12] J. A. Hidalgo-López, J. Romero-Sánchez, and R. Fernández-Ramos, "New approaches for increasing accuracy in readout of resistive sensor arrays," *IEEE Sensors Journal*, vol. 17, no. 7, pp. 2154–2164, 2017.

[13] J. A. Hidalgo-López, O. Oballe-Peinado, and J. A. Sánchez-Durán, "A proposal to eliminate the impact of crosstalk on resistive sensor array readouts," *IEEE Sensors Journal*, vol. 20, no. 22, pp. 13 461–13 470, 2020.

[14] C. Medrano-Sánchez, R. Igual-Catalán, V. H. Rodríguez-Ontiveros, and I. Plaza-García, "Circuit analysis of matrix-like resistor networks for eliminating crosstalk in pressure sensitive mats," *IEEE Sensors Journal*, vol. 19, no. 18, pp. 8027–8036, 2019.

[15] C. Medrano, "Code associated to: Circuit analysis of matrix-like resistor networks for eliminating crosstalk in pressure sensitive mats[source code]," https://codeocean.com/capsule/6185754/tree/v1, 2021.

[16] F. Reverter, F. Vidal-Verdú, and J. A. Hidalgo-Lopez, *Advanced Techniques for Directly Interfacing Resistive Sensors to Digital Systems*. Cham: Springer International Publishing, 2017, pp. 139–165. [Online]. Available: https://doi.org/10.1007/978-3-319-55369-6_4

[17] "Evaluation of measurement data — guide to the expression of uncertainty in measurement," https://www.bipm.org/documents/20126/2071204/JCGM_100_2008_E.pdf, 2008, working Group 1 of the Joint Committee for Guides in Metrology,.

[18] J. Wu, L. Wang, J. Li, and A. Song, "A novel crosstalk suppression method of the 2-d networked resistive sensor array," *Sensors*, vol. 14, no. 7, pp. 12 816–12 827, 2014. [Online]. Available: https://www.mdpi.com/1424-8220/14/7/12816

[19] J. A. Hidalgo-López, O. Oballe-Peinado, J. Castellanos-Ramos, J. A. Sánchez-Durán, R. Fernández-Ramos, and F. Vidal-Verdú, "High-accuracy readout electronics for piezoresistive tactile sensors," *Sensors*, vol. 17, no. 11, 2017. [Online]. Available: https://www.mdpi.com/1424-8220/17/11/2513

[20] J. Wu, L. Wang, and J. Li, "Vf-nse method measurement error analysis of networked resistive sensor array," *Sensors and Actuators A: Physical*, vol. 211, pp. 45–50, 2014. [Online]. Available: https://www.sciencedirect.com/science/article/pii/S0924424714001125

[21] "Evaluation of measurement data — supplement 1 to the "guide to the expression of uncertainty in measurement" — propagation of distributions using a monte carlo method," https://www.bipm.org/documents/20126/2071204/JCGM_101_2008_E.pdf, 2008, accessed: 2021-09-23.

[22] H. Ku, "Notes on the use of propagation of error formulas," *Journal of Research of the National Bureau of Standards*, vol. 70C, no. 4, pp. 263–273, 1966.

[23] W. Li, C. Sun, W. Yuan, W. Gu, Z. Cui, and W. Chen, "Smart mat system with pressure sensor array for unobtrusive sleep monitoring," in *2017 39th Annual International Conference of the IEEE Engineering in Medicine and Biology Society (EMBC)*, July 2017, pp. 177–180.

[24] W. Xu, M. Huang, N. Amini, L. He, and M. Sarrafzadeh, "ecushion: A textile pressure sensor array design and calibration for sitting posture analysis," *IEEE Sensors Journal*, vol. 13, no. 10, pp. 3926–3934, Oct 2013.